Title

MONTHLY PROGRESS REPORT FOR AUGUST. OIL SHALE WASTE TREATMENT: FUNDAMENTAL APPROACHES

Author

Hartstein, Art.

Publication Date

1982-09-03

Lawrence Berkeley Laboratory
UNIVERSITY OF CALIFORNIA

ENERGY & ENVIRONMENT DIVISION

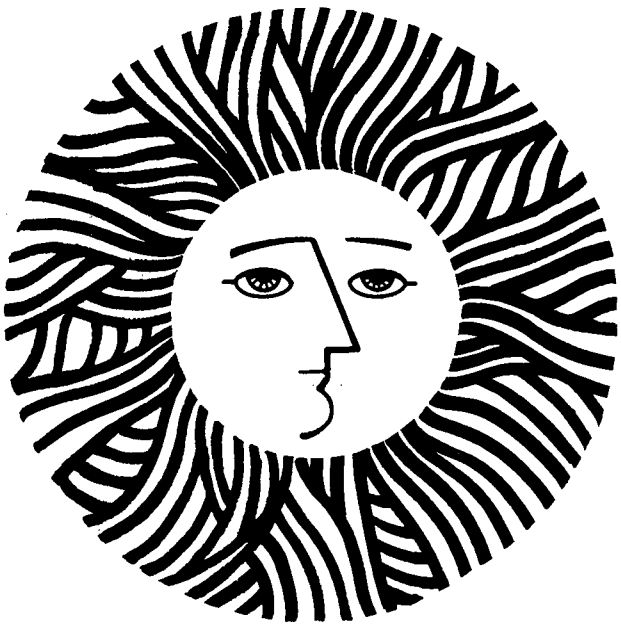

DISCLAIMER

3 September 1982

TO: Art Hartstein

FROM: Bonnie M. Jones, Peter Persoff, Richard H. Sakaji, and Jerome F. Thomas
Lawrence Berkeley Laboratory
University of California, Berkeley
Berkeley, California 94720
and
Christian G. Daughton
Sanitary Engineering and Environmental Health Research Laboratory
University of California, Berkeley
Richmond, California 94804

RE: Monthly Progress Report for August
Oil Shale Waste Treatment: Fundamental Approaches
LBID-605

This work was prepared for the Department of Energy
under Contract No. DE-AC03-76SF0098.

TASK 1. ANALYTICAL METHODOLOGY

Organic Nitrogen Determinations

Previous work comparing the titrimetric with the pyrochemiluminescent method of quantitating ammoniacal nitrogen in sample distillate from Oxy-6 retort water has shown that the two methods of detection give comparable results (July 1982 Monthly Report). This month we began a series of experiments to compare the Kjeldahl method of digestion, distillation, and titration with the pyrochemiluminescent method of nitrogen analysis in raw wastewater samples. This will be done by comparing the recoveries of total nitrogen from nine filtered oil shale process waters and a composite wastewater. The Kjeldahl nitrogen method involves a modified Kjeldahl digestion procedure using selenized Hengar granules, No. 2 Kelpak, and 20 mL sulfuric acid followed by titration (0.025 N sulfuric acid) to a pH 5.4 endpoint. Data from these comparison studies are currently being reduced and will be reported at a future date.

Nitrogen analyses were completed on the nine wastewaters and composite wastewater that were fractionated using the reverse-phase separation procedure

outlined in "Rapid Fractionation of Oil Shale Wastewaters by Reverse-Phase Separation", C.G. Daughton, B.M. Jones, and R.H. Sakaji," (LBID-485; enclosure with February 1982 Monthly Report). The nitrogen content of each fraction was determined by pyrochemiluminescence (Table I). The sums of the values from the hydrophilic and lipophilic fractions (HpF + LpF) were within six percent of the values for the unfractionated samples. These results indicated that only a small percentage of the total nitrogen-containing compounds are irreversibly retained on the C-18 Sep-Paks. Only three waters had LpF nitrogen concentrations in excess of 10 mM. LpF nitrogen is a strong estimator of organic nitrogen and it is interesting that these waters all came from surface retorts (Paraho, 150-Ton, and TV).

The reproducibility of the results for total nitrogen (n = 10) from the Antek nitrogen analyzer was excellent; the relative standard deviations (rsd) for all samples, except TV, were below 2.6 percent. The results from the LpF and HpF (n = 9) were not as precise; the rsd's were below 4.1 percent for all but three of the twenty samples.

The ratios of carbon to nitrogen in the LpF fractions of seven of the oil shale process waters indicate 9 to 14 carbon atoms for every nitrogen atom (Table II). If all of the LpF carbon were associated with nitrogen, then these results are consistent with the theory that the majority of the compounds in the LpF are alkylated N-heterocycles such as pyridines and quinolines.

Ammonia Determination

Nine samples of oil shale wastewater were analyzed for ammonia nitrogen by the phenate colorimetric method (n = 10); all samples were pressure filtered through 0.4-μm polycarbonate membrane filters. These results (Table III) will be included in a Manual of Methods now under preparation. To accomodate the large number of samples, the procedure in the Ammonia Protocol ("Quantitation of Ammonia in Oil Shale Process Wastewaters," LBID-465, December 1981) was modified slightly with no apparent negative effects. Samples were maintained at 0 ^{o}C during preparation prior to heating so that color development in all the samples would occur simultaneously. A short study to compare ammonia analysis by the distillation-titrimetric method to the colorimetric method will be conducted in the near future.

TASK 3. PHYSICOCHEMICAL TREATMENT OF PROCESS WATERS

Steam Stripper

The large fluctuations observed in the temperature of the dry steam were eliminated by modifying the configuration of the associated RTD. The temperature drops were probably caused by the periodic accumulation of condensate on the RTD probe. As a result, the drier supplied excessive heat to the system to compensate for the temperature decrease. Filling the dead space surrounding the probe with silicone sealant stopped the condensation on the probe and reduced observed fluctuations to plus or minus 1 ^{o}C. These fluctuations can probably be reduced further by careful adjustment of the heater voltage and controller bandwidth.

We are currently trying to operate the steam stripper at a ratio of steam to wastewater feed that approaches 1:10. Initial experiments to achieve this ratio were unsuccessful as temperatures in the stripper indicated that the feed preheater was inadequate for heating the larger volume of feed required for this operation.

In an attempt to decrease the steam-to-liquid ratio we first tried to decrease the steam mass flow rate. To achieve the lower steam flow rates, the stripper was operated to minimize the pressure drop through the packed bed. This was accomplished by minimizing the temperature drop between the packed bed and the overheads condenser. Decreasing the steam mass flow rate, however, would also decrease the amount of heat available to compensate for the heat losses through the packed bed. Steam would therefore condense in the packed bed. This resulted in a larger proportion of the steam in the bottoms collector. Condensation in the bottoms also is due, in part, to the heat loss through the bottoms collector. Additional thermocouples were installed to measure the internal temperatures at the cooler ends of the overheads and bottoms collection vessels. There was a 4^{o}C temperature loss through the bottoms collector. The volumetric ratio of overheads to bottoms, without a liquid feed, could be as high as 2:1 for the low steam flow rates. Elimination or reduction of condensation in the bottoms will necessitate heating the bottoms collector.

Task 5. RETORT ABANDONMENT FINAL REPORT

Review comments on the draft report are being incorporated into a final version. A manuscript reporting the results of grout preparation and testing is in preparation for journal publication.

Miscellaneous

C.G. Daughton served as an invited panelist for the Water Management session at the symposium "Oil Shale: The Environmental Challenges III", held at Vail, CO, Aug. 10-12.

P. Persoff attended the Vail Oil Shale Symposium and visited the Colorado Mined Land Reclamation Board and the Colorado Department of Health, Air Quality Section, to review permit applications and obtain data for codisposal scenarios.

Enclosed is a reprint of the paper "An Upstream Finite Element Method for Solution of Transient Transport Equation in Fractured Porous Media" by Jahan Noorishad and Mohsen Mehran was published in Water Resources Research, 1982, 18, 588-596.

Table I. Nitrogen Analysis of Fractionated Wastewater Samples by Pyrochemiluminesence

Process Water		N (mM)	(rsd %)	% of Total
Paraho	total[1]	2448	(1.7)	
	HpF[2]	2284	(6.9)	93.3
	LpF[2]	26	(3.5)	1.1
150-Ton	total	823	(1.8)	
	HpF	815	(0.3)	99.0
	LpF	17	(3.1)	2.1
Oxy-6 GC	total	432	(2.6)	
	HpF	420	(1.7)	97.2
	LpF	4	(2.5)	0.9
S-55	total	323	(2.2)	
	HpF	313	(2.3)	96.9
	LpF	10	(1.8)	3.1
Composite	total	282	(1.5)	
	HpF	262	(4.1)	92.9
	LpF	10	(5.7)	3.6
Omega-9	total	235	(1.6)	
	HpF	229	(1.5)	97.4
	Lpf	5	(2.1)	2.1
TV	total	159	(4.1)	
	HpF	141	(5.3)	88.7
	LpF	12	(2.3)	7.6
Geokinetics	total	144	(2.2)	
	HpF	134	(1.0)	93.1
	LpF	9	(3.6)	6.3
Oxy-6 RW	total	108	(2.0)	
	HpF	95	(1.1)	88.0
	LpF	10	(1.1)	9.3
Rio Blanco Sour	total	67	(1.2)	
	HpF	64	(0.5)	95.5
	LpF	1	(4.1)	1.5

[1] n = 10 for each sample
[2] n = 9 for each sample

Table II. Ratio of LpF Carbon to LpF Nitrogen in Seven Oil Shale Process Waters

Process Water	C (mM)	N (mM)	C/N
150-Ton	174	17	10.2
TV	153	12	12.8
Oxy-6 RW	139	10	13.9
S-55	103	10	10.3
Geokinetics	97	9	10.8
Oxy-6 GC	50	4	12.5
Omega-9	45	5	9.0

Table III. Ammonia Concentrations for Oil Shale Wastewaters (Phenate Colorimetric Method) [1]

Sample	NH_3-N (mg/L)	rsd (%)
Paraho	23,750	0.7
150-ton	11,180	1.1
Oxy-6 gas condensate	6,933	1.0
S-55	4,005	2.0
Omega-9	3,551	4.9
TV	2,346	6.9
Geokinetics	1,505	1.8
Oxy-6 retort water	1,136	0.9
Rio Blanco sour water	1,032	1.1

[1] n = 10 for each sample; J. Cantor; B.M. Jones; R.H. Sakaji; and C.G. Daughton "Quantitation of Ammonia in Oil Shale Process Wastewaters", LBID-465, December 1981.

WATER RESOURCES RESEARCH, VOL. 18, NO. 3, PAGES 588–596, JUNE 1982

An Upstream Finite Element Method for Solution of Transient Transport Equation in Fractured Porous Media

JAHAN NOORISHAD AND MOHSEN MEHRAN[1]

Lawrence Berkeley Laboratory, University of California, Berkeley, California 94720

A finite element method for the solution of two-dimensional transient dispersive-convective transport of nonconservative solute species in fractured porous media is presented. A two-nodal point one-dimensional transport element for fractures is developed which provides a number of advantages relative to conventional fracture representation by two-dimensional continuum elements. To eliminate the oscillatory behavior of convective-dominated transport which is a more likely occurrence in fracture, a very efficient one-dimensional upstreaming method along with a two-dimensional method is implemented. Validity of the numerical scheme is established by comparison with existing one- and two-dimensional analytic solutions.

INTRODUCTION

Solute transport in porous media has been the subject of extensive investigation in the last three decades primarily because of concern over the quality of water supplies [*Lapidus and Amundson*, 1952; *Ogata and Banks*, 1961; *Bredehoeft and Pinder*, 1973; *Sposito et al.*, 1979]. Due to urgent need for developing new energy resources (oil shale, nuclear power, etc.) this concern has recently been intensified to large proportions. Also, with the recognition of the role of fractures in the transport of fluids [*Snow*, 1965; *Wilson and Witherspoon*, 1970], in the face of recent concerns over the safe disposal of hazardous wastes in geologic systems, the problem of contaminant transport in fractured rocks has become the topic of much interest [*Witherspoon et al.*, 1981].

Both analytic and numeric methods have been used to study the transport of nonconservative solute species in fractured porous media. The analytic solutions, although important to the understanding of the fundamental phenomena in solute transport and also necessary for verification of numerical methods, suffer from the usual limitations of initial and boundary conditions plus the restrictions imposed by multidimensionality of transport [*Neretnieks*, 1980; *Rasmuson and Neretnieks*, 1981; *Tang et al.*, 1981]. The numerical solution of *Grisak and Pickens* [1980] on the other hand models the fractures by the two-dimensional continuum elements with different material properties. An attempt is made here to solve the two-dimensional transient transport problem in a fractured porous medium by a novel finite element method, that models the fractures in a discrete fashion by two-nodal point one-dimensional elements developed here. This fracture element not only facilitates the mesh generation and numbering of the elements but greatly enhances the computation efficiency while reducing the requirement of the computer storage capacity.

One of the limitations of the numerical schemes is the oscillation of the concentration profile in situations in which transport is purely convective or convective dominated. Due to high flow velocities in the fractures, the oscillatory behavior of sharp fronts may be more common than in transport through porous media. In the present numerical scheme, two-dimensional and a special one-dimensional upstream weighting functions for the porous matrix and the fracture elements are implemented to prevent such oscillations.

GOVERNING EQUATION

The general governing equation of solute transport in a saturated porous medium in a two-dimensional Cartesian coordinate system is written as

$$L(C) = \frac{\partial}{\partial t}(\theta C + \rho_b S) - \frac{\partial}{\partial x}\left(\theta D_{xx}\frac{\partial C}{\partial x} + \theta D_{xz}\frac{\partial C}{\partial z} - q_x C\right) - \frac{\partial}{\partial z}\left(\theta D_{zx} + \frac{\partial C}{\partial x} + \theta D_{zz}\frac{\partial C}{\partial z} - q_z C\right) - \lambda(\theta C + \rho_b S) - M = 0 \quad (1)$$

where

L	differential operator;
C	concentration in the solution phase, ML^{-3};
ρ_b	bulk density of medium, ML^{-3};
S	amount of solute in the sorbed phase, MM^{-1};
θ	porosity, $L^3 L^{-3}$;
x, z	Cartesian coordinates, L;
t	time, T;
D_{xx}, D_{xz}, D_{zz}	dispersion coefficients, $L^2 T^{-1}$;
q_x, q_z	Darcy velocities, $L T^{-1}$;
λ	first-order reaction constant, T^{-1};
M	source, $ML^{-3} T^{-1}$.

In the above equation, the first term represents the rate of change of total dissolved and adsorbed mass; the second and third terms denote dispersion and advection in the x and z directions, respectively; the fourth term is the mass change due to decay; and finally the term M represents injection or withdrawal rate. In this equation, change of mass as a result of volume changes due to variations of pressure is neglected.

[1] Now at D'Appolonia Consulting Engineers, Inc., Irvine, California 92714.

Paper number 2W0198.
0043-1397/82/002W-0198$05.00

The dispersion tensor D is related to flow field and media properties as [*Bear*, 1972]

$$\theta D_{ij} = (a_T q + D_m \tau)\delta_{ij} + (a_L - a_T)\frac{q_i q_j}{q} \tag{2}$$

where

i, j indicate Cartesian coordinates x, z;
$q = (q_x^2 + q_z^2)^{1/2}$;
a_L, a_T longitudinal and transverse dispersivities;
D_m solute molecular diffusion;
τ tortuosity;
δ_{ij} Kronecker's delta function.

To solve (1), the time rate of change of the adsorbed concentrations must be defined. A common adsorption-desorption model which is a linear equilibrium isotherm, expressed as

$$S = K_d C \tag{3}$$

is assumed where K_d is the distribution coefficient. Substituting (3) in (1) results in a governing equation with only one dependent variable to be solved:

$$L(C) = \theta R_d \frac{\partial C}{\partial t} - \frac{\partial}{\partial x}\left(\theta D_{xx}\frac{\partial C}{\partial x} + \theta D_{xz}\frac{\partial C}{\partial z} - q_x C\right) - \frac{\partial}{\partial z}\left(\theta D_{zx}\frac{\partial C}{\partial x} + \theta D_{zz}\frac{\partial C}{\partial z} - q_z C\right) + \lambda\theta R_d C - M = 0 \tag{4}$$

where

$$R_d = 1 + \frac{\rho_b k_d}{\theta}$$

is the retardation factor which is a measure of the delay of the breakthrough of the dissolved constituent.

As may have been noticed, no reference has yet been made to fractures, and need not be, because the governing equation holds throughout the continuum saturated space of which fractures represent an inhomogeneity with different anisotropic properties. However, if one is concerned with fracture domain only, (4) reduces to

$$L(C) = \theta R_d^f \frac{\partial C}{\partial t} - \frac{\partial}{\partial s}\left(\theta D_{ss}\frac{\partial C}{\partial s} - q_s C\right) + \lambda\theta R_d^f C - M = 0 \tag{5}$$

where s denotes the local uniaxial coordinate system along any fracture and R_d^f represents the fracture retardation factor. Obviously, dispersion and advection in the transverse direction within any fracture are assumed to be negligible. This assumption seems reasonable in view of the fact that both phenomena in the fracture are calculated on the basis of average fracture fluid flow velocity.

Initial and Boundary Conditions

The following provides a set of general initial and boundary conditions:

$$C(x, z, 0) = \hat{C}_0(x, z, 0)$$
$$C(x, z, t) = \hat{C} \text{ on } A_1 \times t[0, \infty) \tag{6a}$$

(Dirichlet boundary condition or first kind)

$$-\left(\theta D_{xx}\frac{\partial C}{\partial x} + \theta D_{xz}\frac{\partial C}{\partial z} - q_x C\right)n_x - \left(\theta D_{zx}\frac{\partial C}{\partial x} + \theta D_{zz}\frac{\partial C}{\partial z} - q_z C\right)n_z = Q(x, z, t) + (\hat{q}_x n_x + \hat{q}_z n_z)C(x, z, t) \text{ on } A_2 \times t[0, \infty) \tag{6b}$$

(Neumann boundary condition or second kind)

$$-\left(\theta D_{xx}\frac{\partial C}{\partial x} + \theta D_{xz}\frac{\partial C}{\partial z} - q_x C\right)n_x - \left(\theta D_{zx}\frac{\partial C}{\partial x} + \theta D_{zz}\frac{\partial C}{\partial z} - q_x C\right)n_z = \hat{Q}(x, z, t) + (\hat{q}_x n_x + \hat{q}_z n_z)\hat{C} \text{ on } A_3 \times t[0, \infty) \tag{6c}$$

(Cauchy boundary condition or third type).

For the fractures the boundary conditions simplify as follows:

$$q_s C = Q_s + \delta(x - x_i, z - z_i)\hat{q}_{s0} C \tag{6d}$$

(Neumann boundary condition)

$$q_s C = \hat{Q}_s + \delta(x - x_i, z - z_i)\hat{q}_{si}\hat{C} \tag{6e}$$

(Cauchy boundary condition) which apply to fracture outflow and inflow points, respectively. In the above equations, n_x and n_z are direction cosines.

A_1, A_2, and A_3 denote different parts of the boundary where various boundary conditions exist. One may note that the difference between the second type and the third type boundary condition is that in the former the amount of solute leaving is concentration dependent and therefore the terms Q, Q_s (the mass inflow or outflow at the boundaries due to diffusion only), and C are unknown quantities as denoted, while in the third type the fluid entering the region has known concentration, and therefore the right-hand side is a known quantity identified by accent marks. The expression $\delta(x - x_i, z - z_i)$ is the dirac delta function which is only nonzero at $x = x_i$, $z = z_i$.

Equation (4) along with the above initial and boundary conditions completely defines the mixed boundary value problem to be solved.

Solution Approach

The complexity of the above convective-dispersive mixed boundary value problem of solute transport inhibits any analytical solution attempts. Recent advances in analytical solution of the simplified transport phenomena problems [*Tang et al.*, 1981] bring valuable contributions to the understanding of solute transport through fractures and accompanied diffusion into the host rock. However, in the more realistic problems, one needs to resort to numerical approaches. In the last few years an increasing number of

numerical schemes have appeared. Recent advances in both finite differences [*Chaudhari*, 1971; *Todd et al.*, 1972] and finite elements [*Heinrich et al.*, 1977; *Huyakorn and Nilkuha*, 1979] have developed to the point of eliminating the numerical oscillations encountered at higher ranges of Peclet number. To our knowledge, all the existing numerical techniques are concerned with only continuum applications. Although these techniques could be applied to fractures by consideration of very thin continuum elements [*Grisak and Pickens*, 1980], practical problems and economical considerations on one hand, and computer storage capacity on the other, may inhibit such applications to fractured media. Additional efforts in mesh generation and numbering and a higher number of nodal points and bandwidth (which greatly exhaust computer storage and time) constitute some of the difficulties in continuum model applications to fractures. Some of these difficulties become even more pronounced in cases where an upstreaming technique is implemented to prevent the oscillatory behavior of the numerical scheme or situations in which one is only concerned with a network of fractures. In the following, an upstream weighted residual finite element method capable of modeling fractures as line elements is presented.

Weighted Residual Finite Element Formulation

Since the formulation and use of upstream finite element methods have been addressed adequately [*Heinrich et al.*, 1977; *Huyakorn and Nilkuha*, 1979], the numerical procedures for the matrix part of the domain of the solute transport problem are given briefly while those concerning fractures will be discussed in detail.

The region of interest R is divided into an assemblage of smaller subdomains called elements. In this work, quadrilateral bilinear isoparametric elements are used for spatial discretization of the porous matrix and one-dimensional line elements for fracture representation. The dependent variable C is approximated in the quadrilateral elements by the relation

$$C \simeq \bar{C} = \sum_{I=1}^{4} N_I C_I \tag{7}$$

where N_I's are known bilinear functions [*Zienkiewicz*, 1977] and C_I's are magnitudes of C at point I. In the line elements the approximation is

$$C \simeq \bar{C} = \sum_{I=1}^{2} N_I C_I \tag{8}$$

where

$$N_I = \frac{1 + \xi\xi_I}{2} \qquad \xi_I = \mp 1 \tag{9}$$

in which ξ is the normalized length of fracture that varies between -1 and $+1$ along the length of the fracture. The weighted residual technique requires that

$$\int_R W_I L[\bar{C}(x, z, t)]\, dR = 0 \tag{10}$$

In the commonly used Galerkin technique, the functions W_I are chosen to be equal to the shape function N_I. However, as discussed earlier, search for a suitable method of preventing oscillation, for cases where advection dominates the dispersion term in the governing equation, has led to selection of special weighting functions which are different from shape functions. An account of related developments as applied to a continuum is given in the work of *Huyakorn and Nilkuha* [1979]. Application of Green's second theorem to (10) and integrating over subregions yields

$$A_{IJ}C_J + M_{IJ}\frac{dC_J}{dt} + G_I = 0 \tag{11}$$

This expression when given in terms of subregion contributions of m quadrilateral elements and $N - m$ fracture elements becomes

$$\left[\sum_{1}^{m} A_{IJ}{}^{pe} + \sum_{m+1}^{N} A_{IJ}{}^{fe}\right]C_J + \left[\sum_{1}^{m} M_{IJ}{}^{pe} + \sum_{m+1}^{N} M_{IJ}{}^{fe}\right]\frac{dC_J}{dt} + [G_I{}^{pe} + G_I{}^{fe}] = 0 \tag{12}$$

where A_{IJ}, M_{IJ} and G_I are diffusion-advection, storage, and source matrices, respectively. Details of these terms for continuum elements, designated by *pe* here, are common knowledge and only for the sake of completeness are given in the appendix. Also, as it is known, evaluation of continuum element matrices are done normally by Gauss's quadrature method. However, the details of the corresponding terms for two-nodal point elements of fractures are developed and the closed form results are presented:

$$A_{IJ}{}^{fe} = 2b\theta D_{ss}\int_{Se}\frac{\partial W_I}{\partial s}\frac{\partial N_J}{\partial s}ds - 2bq_s \cdot \int_{Se}\frac{\partial W_I}{\partial s}N_J ds + \delta(J-2)2bq_{s0} + 2b\theta\lambda R_d{}^f\int_{Se} W_I N_J ds \tag{13}$$

$$M_{IJ}{}^{fe} = 2b\theta R_d{}^f\int_{Se} W_I N_J ds$$

$$G_I{}^{fe} = \delta(x - x_i)\delta(z - z_i)q_{si}C$$

where I and J assume values of 1 and 2 and i designates the fracture inflow point. The term Se refers to the surface of a fracture element in the domain of interest R. The last term of the $A_{IJ}{}^{fe}$ term represents the contribution of the Neumann type boundary condition at node 2 of any fracture of $2b$ width, when it is being treated implicitly. At this point we draw attention to (6), which provides the most general conditions that can arise in transport problems. In considering transport problems in porous media only, the Neumann boundary condition is simplified by neglecting the $Q(x, z, t)$ term. This is justified by the fact that the dispersive transport at the boundary is much smaller than the advective transport represented by the second term. Therefore, in the finite element formulation of the porous continuum, only the proper contribution of the advective term is introduced (see appendix). The Cauchy type boundary condition for porous media is normally lumped into a single known mass inflow term represented by the G_I term in the finite element

formulation. The choice between the latter treatment of Cauchy type boundary condition and its representation by a Dirichlet type boundary condition, which assumes the concentration of the inflow solute as constant boundary value, although they are not equivalent, is not straightforward and is subjective.

In case of the existence of fractures, the Cauchy type boundary condition can be treated similarly for fracture boundary intersections. However, the treatment of Neumann type boundary conditions, as explained above, may not always hold true for fracture boundaries. This is because, in case of high dispersivity fractures, important mass transport to the outside environment can also take place by dispersion. In the numerical treatment it is very difficult if not impossible to account accurately for this concentration dependent dispersive outflow. The problem lies in the determination of gradient and definition of dispersivity at the boundary point. Employing the local isoparametric one-dimensional element and using the following weighing functions [*Huyakorn and Nilkuha*, 1979]

$$W_1 = \tfrac{1}{4}[(1+\xi)(3\alpha\xi - 3\alpha - 2) + 4]$$
$$W_2 = \tfrac{1}{4}[(1+\xi)(-3\alpha\xi + 3\alpha + 2)] \tag{14}$$

where

$$\alpha_{opt} = \coth\left(\frac{\beta}{2}\right) - \frac{2}{\beta} \tag{15}$$

and

$$\beta = \frac{q_s l}{D_{ss}} \tag{16}$$

the closed form for the fracture integral expressions is obtained as:

$$[A_{IJ}{}^{fe}] = \frac{2b\theta D_{ss}}{l}\begin{bmatrix} 1 & -1 \\ -1 & 1 \end{bmatrix} + \frac{2bq_s}{2}\begin{bmatrix} -(1+\alpha) & -(1-\alpha) \\ (1+\alpha) & (1-\alpha) \end{bmatrix} \tag{17}$$

$$[M_{IJ}{}^{fe}] = \frac{2bl\theta}{6}\begin{bmatrix} (2-\alpha/4)\,(1-\alpha/4) \\ (1+\alpha/4)\,(2+\alpha/4) \end{bmatrix}$$

In the above expressions, β is the fracture Peclet number and l is the fracture length. Equation (15) for optimum α (α_{opt}) is given by *Christie et al.* [1976].

Time integration of (11) is done by the mid-difference finite difference scheme. In this method the values of the unknown are assumed to vary linearly with time in the time interval Δt. The recurrence formula thus is of the following form:

$$\left[\frac{2}{\Delta t}M_{IJ} + A_{IJ}\right]C_J{}^{t+\Delta t/2} - \frac{2}{\Delta t}M_{IJ}C_J{}^{t} + G_I = 0 \tag{18}$$

$$C_J{}^{t+\Delta t} = 2C_J{}^{t+\Delta t/2} - C_J{}^{t}$$

COMPUTER CODE

A Fortran IV program for numerical algorithm of (12) was prepared. In effect, the convective dispersive code forms part of a complete finite element fluid flow and transport code called 'flows' for saturated fractured porous media. The code first solves the fluid flow problem in the region of interest and through the use of an auxilliary finite element routine calculates velocities at the nodal points of the continuum elements. This smooths out the velocity distribution of the linear quadrilateral elements and ensures continuity of velocity across element boundaries. Nodal point velocities are also required for the upstream scheme referred to earlier. Fracture element velocities are calculated directly from endpoint pressures. This average fracture velocity, in view of ambiguity of fracture nodal point velocities, is best suited for calculation of convective matrices and also for upstream calculations. In the second phase the code solves the transport problem using the previously calculated velocities. This part of the code reuses the fluid flow storage space, but due to the nonsymmetric nature of resulting matrix equations it employs its own nonsymmetric solver. Developments of fluid flow analysis are assumed common knowledge and are not given here.

VERIFICATION

To illustrate the validity and accuracy of the numerical scheme and also to demonstrate the influence of upstream weighting functions on the oscillatory behavior in discrete fractures, the transient diffusive convective equation with simplified initial and boundary conditions is used.

One-Dimensional Transport in Discrete Fractures

As mentioned earlier, one of the advantages of the present scheme is the capability of handling only discrete fractures, using two-nodal point elements. Figure 1 shows a fracture with length 10 divided into 20 elements.

To check the validity of the numerical scheme, the results were compared with those obtained from the diffusion convection equation of the following form:

$$\frac{\partial C}{\partial t} = D\frac{\partial^2 C}{\partial x^2} - v\frac{\partial C}{\partial x} \tag{19}$$

where v is the average pore water velocity defined as the ratio of Darcy velocity to porosity.

The appropriate initial and boundary conditions for the problem considered are written as

$$C(x, 0) = 0 \tag{20a}$$

$$C(\infty, t) = 0 \tag{20b}$$

$$C(0, t) = C_0 \tag{20c}$$

Defining the mesh Peclet number (Pe) as

$$Pe = \frac{v\Delta x}{D}$$

where Δx is the space increment along the fracture. (5) subject to (20) is solved using numerical values of $\Delta x = 0.5$, $v = 0.5$, and $D = 0.025$ corresponding to $Pe = 10$ which are the same as those used by *Huyakorn and Nilkuha* [1979]. The concentration profile in the fracture at $t = 6.4$ is shown in Figure 2 and compared to the exact solution of (19) ex-

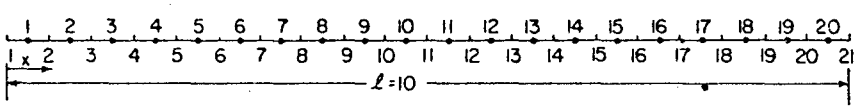

Fig. 1. Schematic diagram of a fracture with two-nodal point element representation.

pressed as:

$$\frac{C}{C_0} = \frac{1}{2}\left[\operatorname{erfc}\left\{\frac{x - vt}{2(Dt)^{1/2}}\right\} + \exp\left(\frac{vx}{D}\right) \cdot \operatorname{erfc}\left\{\frac{x + vt}{2(Dt)^{1/2}}\right\}\right] \quad (21)$$

The comparison between the numeric (points) and analytic (solid line) results shows that for small Peclet numbers, the numerical scheme gives satisfctory answers. It should be pointed out that the same problem was modeled using a row of 20 four-nodal point elements with the same spacing. The results matched exactly (Figure 2) those of the two-nodal point element model.

Upstream Weighting Functions

In situations where the transport is purely convective or convective dominated (large Peclet numbers), the finite element numerical solutions exhibit strong oscillatory behavior. To demonstrate this behavior, a $Pe = 100$ was selected for the previous problem assuming other parameters remain the same. The oscillation of the concentration profile as compared to the analytic solution is shown in Figure 3. The numerical solution is not only oscillatory but considerably more dispersed in the downstream portion of concentration profile. Using weighting functions (14), the oscillations can be minimized as shown in Figure 3 by implementing α_{opt} given by (15). These results are exactly the same as those obtained by *Huyakorn and Nilkuha* [1979].

Transport in Fracture and Transverse One-Dimensional Diffusion in the Porous Matrix

To confirm the validity of the numerical scheme for solute transport in a fractured porous continuum, the analytic solution of *Tang et al.* [1981] and the modeled region of *Grisak and Pickens* [1980] are utilized. The primary reason for these selections are that the analytic solution of *Tang et al.* [1981] accounts for diffusion from the fracture into the matrix and that they have compared their results to the numerical solution of *Grisak and Pickens* [1980].

Figure 4 illustrates the schematic diagram of the observation segment of the modeled region and its appropriate discretization in x and z directions. To simulate correct behavior for the observation length of the model which is 0.76 m, the required length of the model in view of the data used and the observation period involved, is at least three times the observation length as noted by *Grisak et al.* [1980]. The width of the model selected in accordance with that of *Grisak and Pickens* [1980] is 2 cm. This length can simulate infinity in the x direction for the range of dispersion coefficients used for the porous matrix. As may be noted, the fracture in this model is represented by the string of two-nodal point elements which coincide with the side of the first column of four-nodal point porous matrix elements. In this representation of fractures, only average fracture velocity is used in each fracture element.

The general initial and boundary conditions for the fractured porous continuum as shown in Figure 4 are as follows:

$$C(z, x, 0) = 0 \quad (22a)$$

$$C(z, x, t)_{\substack{t>0 \\ z=0}} = \hat{C}_0 \quad (22b)$$

$$\frac{\partial C}{\partial z}(z, x, t)_{z=l} = 0 \quad (22c)$$

$$\frac{\partial C}{\partial x}(z, x, t)_{x=d} = 0 \quad (22d)$$

where d is the width of the matrix block. The model is verified with the analytic solution (equation (35) of *Tang et al.* [1981]) describing solute transport in the fracture considering diffusion into the matrix.

The parameters given below were the same as those used by *Grisak and Pickens* [1980] and also by *Tang et al.* [1981]:

$$2b = 120\ \mu\text{m}$$

$$\theta = 0.35$$

$$a_L = 0.76\ \text{m}$$

$$v = 0.75\ \text{m/d}$$

The diffusion coefficient D_{zz} is assumed to be zero and the diffusion coefficient D_{xx} in the matrix is varied from 0 to 10^{-6} cm^2/s. The concentration profiles in the fracture at the end of 4 days are shown in Figure 5. The points represent the finite element solution while the solid lines denote the analytical solution. The agreement between the two solutions is generally very good. There is some disrepancy between the two solutions for the medium range of diffusion coefficients. Closer inspection of the curves reveal the largest discrepancy at around D_{xx} of 10^{-7} cm^2/s and 10^{-8} cm^2/s which rapidly falls off for lower diffusion coefficients. The differences are caused by the coarseness of the mesh which dampens the effect of the very high gradients that develop in the medium range of the dispersion coefficients. Therefore diffusive

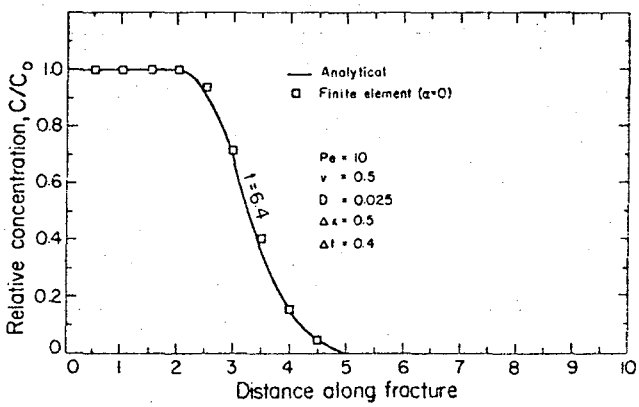

Fig. 2. Concentration profiles at $t = 6.4$ comparing analytic and numeric solutions for $Pe = 10$ in the fracture.

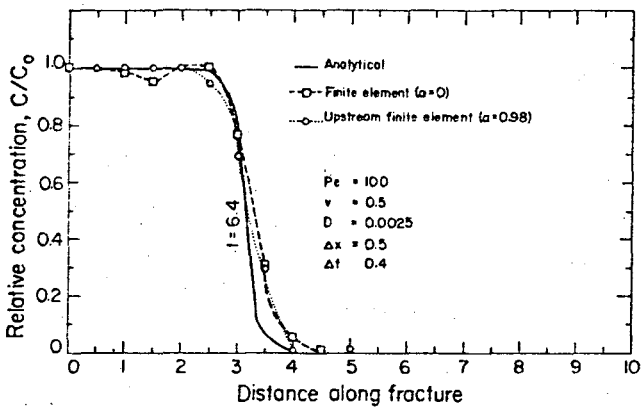

Fig. 3. Concentration profiles at $t = 6.4$ comparing analytic, numeric, and upstream FE solutions.

losses are reduced, and consequently the numerical results plot above the analytical solution. In the lower ranges of the diffusion coefficients, diffusive losses are too small to be affected by misrepresentation of gradient due to the coarseness of the mesh.

Figure 6 illustrates the concentration profiles with time in the fracture at 0.76 m from the source. The agreement between numeric and analytic solutions for early times seems satisfactory for most cases. In the absence of the porous matrix, i.e., $D = 0$, the numerical results match perfectly those of the analytical solution. This indicates optimum discretization in time and space (z direction only) for transport equation in the fracture. Also truncation errors, for higher diffusion coefficients of the porous matrix, stay in reasonable range for the observation time considered. Based on this behavior of the problem, the major early time disrepancy in the case of $D = 10^{-10}$ cm^2/s for the porous matrix could be attributed mainly to the lack of required mesh refinement in the x direction. Few trials with reduced time steps and a reduced mesh (obtained from compression of the original mesh) improved the early time results favorably. However, a sensitivity analysis for the small range of porous matrix diffusion values was not performed in view of clearness of the obtained result. The comparison between the analytic solution of *Tang et al.* [1981] and the numeric solution of *Grisak and Pickens* [1980] shows that in the middle ranges of diffusion coefficients (10^{-8} to 10^{-9} cm^2/s) considerable amount of discrepancy exists as shown by *Tang et al.* [1981]. They attribute these discrepancies to the errors resulting from insufficient discretization in the numerical solution near the fracture interface. The reason for the numerical solutions, in this case, plotting below the analytical solutions may lie in the fully implicit backward difference time discretization scheme that was utilized. Considering the better results obtained here for the case of $D = 10^{-10}$ cm^2/s, as compared to our results for the same case, one may note that the mid-difference scheme used in our developments, as might be expected, is not responsive to the rapidly varying field variable in early times. However, convergence to the true solution and better late time results as seen in Figures 5 and 6 makes the latter scheme more advantageous as noted by *Gureghian et al.* [1980]. It should also be mentioned that although implementation of most of the generally used difference schemes is a simple matter, it was not the goal of this work to pursue it.

Transport in Fracture and Two-Dimensional Diffusion in the Porous Matrix

The absorptive capacity of the porous matrix as suggested by *Tang et al.* [1981] coud act as a safety mechanism in potential contamination problems. This absorptive capacity not only depends on diffusive properties of the fracture and the medium but is a function of fracture fluid velocity and porous matrix porosity. To illustrate the point, the example of *Grisak and Pickens* [1980] for $D_m = 1 \times 10^{-6}$ cm^2/s and various fracture fluid velocities and matrix porosities is worked out. The concentration profiles in the fracture at 0.2

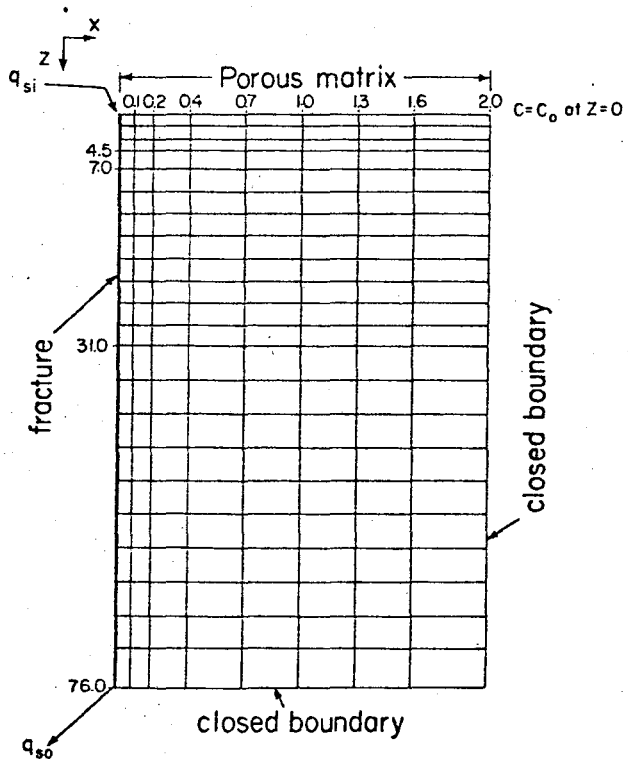

Fig. 4. Schematic diagram of the observation segment of the modeled region for two-dimensional solute transport (actual mesh extends to 234 cm). Dimensions are in centimeters.

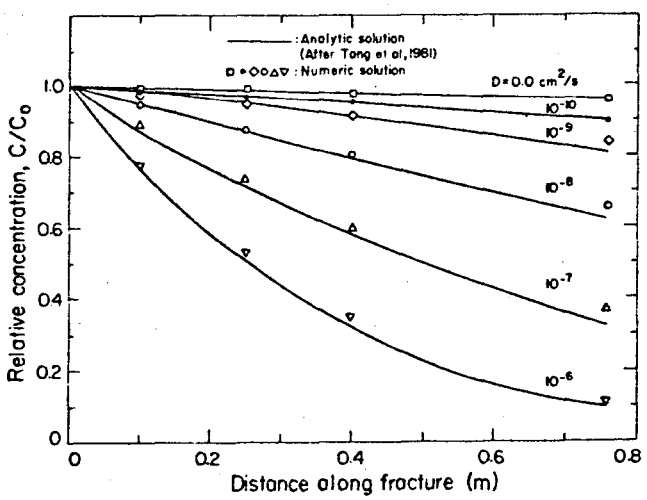

Fig. 5. Comparison between analytic solution of *Tang et al.* [1981] and numeric solution at 4 days.

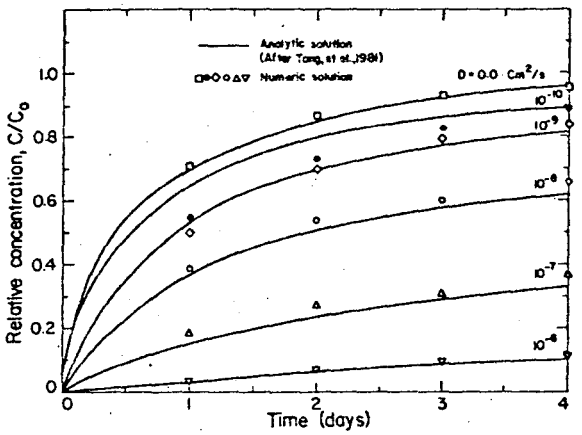

Fig. 6. Comparison between analytic solution of *Tang et al.* [1981] and numeric solution for breakthrough curves for fracture at 0.76 m from the source.

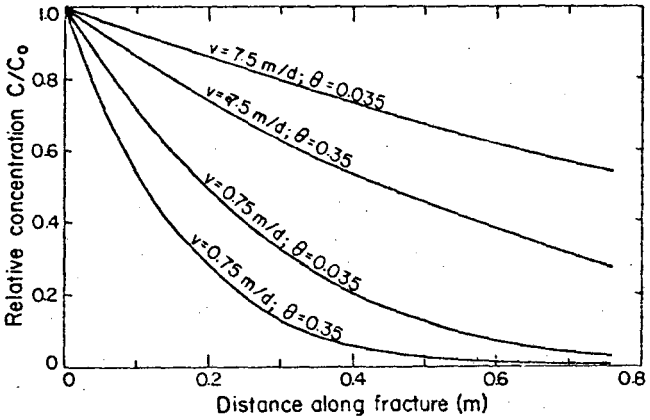

Fig. 7. Concentration profiles in the fracture at 0.2 day for various fracture velocities and matrix porosities. Matrix diffusion coefficient is assumed to be 1×10^{-6} cm²/s.

day are shown in Figure 7. As fracture fluid velocity increases, less time is allowed for diffusion into the matrix, and therefore higher concentrations in the fracture are observed. Figure 7 also shows that the effect of matrix porosity is more pronounced at higher fluid velocity. Highest absorptive capacity is attained at low fracture fluid velocity and high matrix porosity.

In comparing the results with analytic solution of *Tang et al.* [1981], we also assumed that concentration gradient is perpendicular to the fracture. This was in accordance with the assumption of orthogonality in deriving the analytic expression by *Tang et al.* [1981]. Although this assumption may be valid and at early times the influence of diffusion in the other dimension might be insignificant, neglecting two dimensionality of flow for long-term real problems or simulations may cause serious errors. To illustrate this point, the previous problem for the case of $D_{zz} = 1 \times 10^{-6}$ cm²/s is solved and compared to the case which D_{zz} was assumed to be zero. The result for concentration profiles in the fracture and also in the matrix at 0.1 cm from the fracture is given in Table 1. Higher relative concentrations are observed when diffusion takes place in two dimensions. The effect is more pronounced in the beginning of the fracture where concentrations are generally higher. The difference between the two cases is even more pronounced for the porous matrix near the source. It is believed that for long-term problems of interest, two dimensionality of diffusion may play a significant role and therefore cannot be ignored.

CONCLUSIONS

In this paper we have considered the problem of two-dimensional transient transport of solutes in fractured porous media using an upstream finite element scheme. The processes of advection, dispersion, diffusion, adsorption, and first-order reaction in the fracture and porous matrix are included in the mathematical model.

The numerical algorithm first solves the fluid flow problem in the region of interest and then by an auxilliary finite element routine the nodal point velocities of the continuum elements are determined. This procedure not only ensures continuity of velocity across element boundaries, but it is also required for implementation of upstream weighting functions. Fracture element velocities are average velocities calculated directly from endpoint pressures. Knowing the fluid flow field, the code then solves the transport equation using its own nonsymmetric solver.

One of the unique features of this study is the representation of discrete fractures by two-nodal point elements. This not only facilitates the mesh generation and numbering of the elements, but greatly enhances the computation efficiency and reduces the required computer storage.

To check the validity and accuracy of the numerical scheme, one-dimensional advective diffusive transport of a conservative solute species in the fracture was solved for a small Peclet number, and the results were compared with those obtained from appropriate analytic solutions. The

TABLE 1. Concentration Profiles in the Fracture and in the Porous Matrix (0.1 cm From Fracture) at 4 Days Illustrating the Effect of Diffusion in the Second Dimension in the Matrix

Distance From Source, cm	$D_{zz} = 0$; $D_{xx} = 1 \times 10^{-6}$		$D_{zz} = 1 \times 10^{-6}$; $D_{xx} = 1 \times 10^{-6}$	
	Fracture	Matrix	Fracture	Matrix
0.0	1.00000	1.00000	1.00000	1.00000
1.5	0.96598	0.91204	0.96649	0.93227
3.0	0.93261	0.87952	0.93325	0.88286
4.5	0.90004	0.84790	0.90067	0.84820
7.0	0.84774	0.79715	0.84834	0.79777
10.0	0.78805	0.73942	9.78862	0.73998
31.0	0.35624	0.37266	0.35655	0.37299
76.0	0.11965	0.12463	0.11977	0.12476

agreement between the two is satisfactory (Figure 2). Since, due to high flow velocities and low dispersivities, the solute transport in the fracture could be purely convective or convective dominated, special upstream weighting functions are formulated and implemented in the numerical scheme in order to prevent the oscillatory behavior of concentration profiles (Figure 3). The results are in agreement with those obtained by previous workers for a porous continuum.

Validation of the numerical scheme for solute transport in the fracture with the diffusive losses into the matrix is performed by comparing the results to the analytic solution presented by *Tang et al.* [1981]. The agreement between the two results is generally good for the times considered. Small discrepancies at early times when the diffusion coefficient in the porous matrix is extremely small (1×10^{-10} cm^2/s) are attributed to the numerical approximations involved in estimation of solute flux into the matrix as a result of coarseness of the mesh and largeness of the time steps through the insensitive nature of the mid-difference scheme used in our development.

It is also demonstrated that the velocity of flow in the fracture and porosity of the matrix play a dominant role in the absorptive capacity of the porous matrix. Highest retardation is obtained at low fracture fluid velocity and high matrix porosity.

Inclusion of two-dimensional diffusive transport in the porous matrix illustrates that at early times one-dimensional solute diffusion perpendicular to the fracture does not cause serious errors, while for long-term problems (i.e., radionuclide transport) we may encounter significant differences and two dimensionality of diffusion in the porous matrix may have a pronunced effect on concentration profiles particularly in the vicinity of the source.

APPENDIX

The diffusion-advection, storage, and source matrices for the porous elements as defined in (12) are expressed as

$$A_{IJ}^{Pe} = \left\{ \int_{Re} \frac{\partial W_I}{\partial x} \left[\theta D_{xx} \frac{\partial N_J}{\partial x} + \theta D_{xz} \frac{\partial N_J}{\partial z} - q_x N_J \right] + \frac{\partial W_I}{\partial z} \left[\theta D_{zx} \frac{\partial N_J}{\partial x} + \theta D_{zz} \frac{\partial N_J}{\partial z} - q_z N_J \right] \right\} dR + \lambda \theta R_d \int_{Re} W_I N_J dR$$

$$M_{IJ}^{Pe} = \theta R_d \int_{Re} W_I N_J \, dR$$

$$G_I^{Pe} = \int_{A3e} W_I \left\{ - \left[\theta D_{xx} \frac{\partial \hat{C}}{\partial x} + \theta D_{xz} \frac{\partial \hat{C}}{\partial z} - \hat{q}_x \hat{C} \right) \right] n_x + \left[- \theta D_{zk} \frac{\partial \hat{C}}{\partial x} - \theta D_{zz} \frac{\partial \hat{C}}{\partial z} + \hat{q}_z \hat{C} \right] n_z \right\} dA$$

The last integral represents the Cauchy boundary conditions. The treatment of Neumann type boundary conditions, if done explicitly, can be accomplished like the Cauchy boundary condition explained in G_I. Full implicitness of the Neumann boundary condition can be brought about by either iterations, until convergence, on the results of the explicit treatment or a one-step fully implicit treatment as shown for the fracture. In the latter case the following contribution needs to be added to the A_{IJ} matrix of the porous elements where this boundary condition prevails

$$A_{IJ}^{Pe} = A_{IJ}^{Pe} + E_{IJ}^{Pe}$$

where

$$E_{IJ}^{Pe} = \int_{A2e} W_I [v_x n_x + v_z n_z] N_J \, dA$$

Note that the diffusion part of the Neumann boundary condition is not considered because the contribution is normally negligible. Also the other source terms in the above presentation have not been included to make presentation simple. Upstream finite element treatment of porous media, as mentioned earlier, has been adequately explained in other publications and repetition is avoided.

Acknowledgments. This work was supported by the Director, Office of Energy Research, Office of Basic Energy Sciences, Division of Engineering, Mathematics and Geosciences, and by the Assistant Secretary for the Environment, Office of Environmental Compliance and Overview, Environmental Control Technology Division, and the Assistant Secretary for Fossil Energy, Office of Oil Shale, of the U.S. Department of Energy, under contract DE-AC03-76SS00098.

REFERENCES

Bear, J., *Dynamics of Fluids in Porous Media*, 764 pp., Elsevier, New York, 1972.

Bredehoeft, J. D., and G. F. Pinder, Mass transport in flowing groundwater, *Water Resour. Res.*, *9*(1), 194–210, 1973.

Chaudhari, N. M., An improved numerical technique for solving multidimensional miscible displacement equations, *Soc. Pet. Eng. J.*, *11*, 277–284, 1971.

Christie, I., D. F. Griffiths, A. R. Mitchell, and O. C. Zienkiewicz, Finite element methods for second order differential equations with significant first derivatives, *Int. J. Numer. Methods Eng.*, *10*, 1389–1396, 1976.

Grisak, G. E., and J. F. Pickens, Solute transport through fractured media, 1, The effect of matrix diffusion, *Water Resour. Res.*, *16*(4), 719–730, 1980.

Grisak, G. E., J. F. Pickens, and J. A. Cherry, Solute transport through fractured media, 2, Column study of fractured till, *Water Resour. Res.*, *16*(4), 731–739, 1980.

Gureghian, A. B., D. S. Ward, and R. W. Cleary, A finite element model for migration of leachates from a sanitary landfill in Long Island, New York, Part I, Theory, *Water Resour. Bull.*, *16*(5), 900–906, 1980.

Heinrich, J. C., P. S. Huyakorn, O. C. Zienkiewicz, and A. R. Mitchell, An upwind finite element scheme for two-dimensional convective transport equation, *Int. J. Numer. Methods Eng.*, *11*, 131–143, 1977.

Huyakorn, P. S., and K. Nilkuha, Solution of transient transport equation using an upstream finite element scheme, *Appl. Math. Model.*, *3*, 7–17, 1979.

Lantz, R. B., Quantitative evaluation of numerical diffusion (truncation error), *Soc. Pet. Eng. J.*, *10*, 315–320, Sept. 1970.

Lapidus, L., and N. R. Amundson, Mathematics of adsorption in beds, *J. Phys. Chem.*, *56*, 984–988, 1952.

Neretnieks, I., Diffusion in the rock matrix: An important factor in radionuclide retardation, *J. Geophys. Res.*, *85*, 4379–4397, 1980.

Ogata, A., and R. B. Banks, A solution of the differential equation of longitudinal dispersion in porous media, *U.S. Geol. Surv. Prof. Pap.*, *411-A*, 1961.

Rasmuson, A., and I. Neretnieks, Migration of radionuclides in fissured rock: The influence of micropore diffusion and longitudinal dispersion, *J. Geophys. Res.*, *86*(B5), 3749–3758, 1981.

Snow, D. T., A parallel plate model of fractured permeable media, Ph.D. thesis, Univ. of Calif., Berkeley, 1965.

Sposito, G., V. K. Gupta, and R. N. Bhattacharya, Foundation theories of solute transport in porous media: A critical review, *Adv. Water Resour.*, *2*(2), 59–68, 1979.

Tang, D. H., E. O. Frind, and E. A. Sudicky, Contaminant transport in fractured porous media: Analytic solution for a single fracture, *Water Resour. Res.*, *17*(3), 555–564, 1981.

Todd, M. R., P. M. O'Dell, and G. J. Hirasaki, Methods for increased accuracy in numerical reservoir simulators, *Soc. Pet. Eng. J.*, *12*, 515–530, 1972.

Wilson, C. R., and P. A. Witherspoon, An investigation of laminar flow in fractured porous rocks, *Publ. 70-6*, Dep. of Civ. Eng., Univ. of Calif., Berkeley, 1970.

Witherspoon, P. A., N. G. W. Cook, and J. E. Gale, Geologic storage of radioactive waste: Field studies in Sweden, *Science*, *211*, 894–900, 1981.

Zienkiewicz, O. C., *The Finite Element Method*, 3rd ed., McGraw-Hill, New York, 1977.

(Received November 5, 1981;
revised January 20, 1982;
accepted February 3, 1982.)

This report was done with support from the Department of Energy. Any conclusions or opinions expressed in this report represent solely those of the author(s) and not necessarily those of The Regents of the University of California, the Lawrence Berkeley Laboratory or the Department of Energy.

Reference to a company or product name does not imply approval or recommendation of the product by the University of California or the U.S. Department of Energy to the exclusion of others that may be suitable.

TECHNICAL INFORMATION DEPARTMENT
LAWRENCE BERKELEY LABORATORY
UNIVERSITY OF CALIFORNIA
BERKELEY, CALIFORNIA 94720